A web-based interface for modeling laser-induced incandescence (LIISim)

M. Hofmann*, B. Kock, C. Schulz

IVG, University of Duisburg-Essen, Duisburg, Germany

Abstract

In this study we present a simulation tool, called LIISim, for simulating laser-induced incandescence (LII). Different heat conduction models can be selected and mono- or polydisperse particles can be chosen as well as isolated, single particles or aggregates. We present a web interface that allows the scientific community to directly use this simulation tool. This will simplify the comparison of LII models developed by different research groups. The web interface of LIISim is available at http://www.liisim.com.

Introduction

LII has been used over the past 20 years to determine both soot concentrations and soot particle sizes in the sub-micron region. Recently, the focus in LII has been on the measurement of primary particle sizes of soot. The production of ultra-fine soot particles in the range of 5–100 nm by combustion is of major concern for health risks as these particles are considered to cause cancer, asthma, allergies and fibrosis.

In LII, nano-sized particles are heated by a pulsed laser of several nanoseconds duration after which they cool down until they reach their initial temperature again. The signal is due to the thermal radiation of the laser-heated particles. In order to obtain particle sizes from experimental LII signal decays, numerical models are required that describe the cooling process after laser heating. These models are fitted to experimental data with the particle size or both the mean diameter and the geometric width of a particle-size distribution as free parameters. Modeling the LII process is of major importance when applying LII for sizing of nano-particles and much progress has been made on modeling the relevant heat- and mass-loss mechanisms. However, significant discrepancies exist between the models developed by different research groups [1,2]. The goal of this work is to simplify the comparison of other LII models with the results of the simulation tool developed in this study. Therefore, several recent developments and improvements in modeling the heat- and mass transfer in LII were incorporated in a computer program, called LIISim. It was made available to the scientific community by a web interface. This will not only facilitate the comparison between LIISim results and other LII simulations, but will enable the evaluation of experimental LII signals via the internet.

In the following, the underlying physics of LIISim will be explained for the case of soot particles and the web interface for modeling and fitting of experimental data will be described.

Specific Objectives

The incandescence of particles is induced by a laser of several nanoseconds duration. Depending on the laser fluence, soot particles are heated up to 2000 – 4000 K and cool down over a period of some hundreds of nanoseconds. The absolute light intensity of the incandescence is related to the soot volume fraction, whereas the signal decay correlates to the particle size, as small particles cool down faster than large particles.

Numerous models have been developed [3-9] to predict the temporal behavior of the LII signal. The basis for most models is an energy and mass balance that considers the absorption of laser energy as well as heat loss due to vaporization of material from the surface, heat conduction to the surrounding gas, and radiation. This energy balance can be written as

$$\dot{Q}_{\mathrm{abs}} = \dot{Q}_{\mathrm{int}} + \dot{Q}_{\mathrm{evap}} + \dot{Q}_{\mathrm{cond}} + \dot{Q}_{\mathrm{rad}} \qquad (1)$$

where $\dot{Q}_{\mathrm{abs}}$ is the energy flux of laser absorption, $\dot{Q}_{\mathrm{int}}$ is the change in internal energy, $\dot{Q}_{\mathrm{evap}}$ is the energy flux due to evaporation, $\dot{Q}_{\mathrm{cond}}$ the energy flux related to heat conduction and $\dot{Q}_{\mathrm{rad}}$ the heat loss due to radiation. A more detailed model for soot particles including thermal annealing and oxidation has been developed by Michelsen [10]. If the laser energy is sufficient to heat the particle above the vaporization threshold, carbon fragments will evaporate from the particle surface which will result in a mass loss of the particle and an increase of mass in the gas phase. This mass balance is described as

$$\mathrm{d}m_{\mathrm{p}} / \mathrm{d}t = J_{\mathrm{evap}} \qquad (2)$$

with the particle mass m_{p}, the time t and the mass flux J_{evap}. The resulting coupled differential equation given by the equations (1) and (2) can be solved numerically and yields the particle temperature and particle diameter as a function of time. The particle temperature is then turned into LII signal intensities using Planck's law.

Specific heat and mass balance of LIISim

The detailed expressions for the different heat- and mass-loss mechanisms used in LIISim will be given in the following section. LIISim allows to choose between different sub-models, e.g. for the heat conduction or aggregation.

* Corresponding author: maximilian.hofmann@uni-due.de

Absorption

The absorption of laser light by the particle is given by

$$\dot{Q}_{\mathrm{abs}} = C_{\mathrm{abs}} F(t) \tag{3}$$

The temporal intensity profile of the laser is given by the function *F(t)* and is assumed to be Gaussian with 7 ns FWHM, a typical value for Q-switched Nd:YAG lasers. On the other hand, experimentally-measured laser profiles can be applied for *F*(*t*). The spatial intensity profile of the laser is assumed to be rectangular, i.e. the fluence within the probe volume is homogeneously distributed and all particles are heated by the same laser fluence. If the particle is small compared to the laser wavelength, i.e. $\pi d_{\mathrm{p}}/\lambda < 0.3$, the absorption cross-section is given by

$$C_{\mathrm{abs}} = \frac{\pi^2 d_p^3}{\lambda_{\mathrm{ex}}} E(m) \tag{4}$$

where d_{p} is the primary particle diameter, λ_{ex} is the excitation wavelength and *E(m)* is the soot-absorption function of the complex index of refraction [11].

Change in internal energy

The change in internal energy is given by

$$\dot{Q}_{\mathrm{int}} = \frac{\mathrm{d}\left(m_{\mathrm{p}} c_{\mathrm{p,s}} T_{\mathrm{p}}\right)}{\mathrm{d}t} \tag{5}$$

where T_{p} is the particle temperature. The heat capacity of soot $c_{\mathrm{p,s}}$ is expressed empirically in dependence on the particle temperature:

$$c_{\mathrm{p,s}} = \frac{a_{\mathrm{c,s}} + b_{\mathrm{c,s}} T_{\mathrm{p}} + c_{\mathrm{c,s}} / T_{\mathrm{p}}^2}{M_{\mathrm{s}}} \tag{6}$$

where $a_{\mathrm{c,s}}$, $b_{\mathrm{c,s}}$ and $c_{\mathrm{c,s}}$ are empirical constants and M_{s} is the molar mass of graphite [9]. It should be noted that most models in literature use the expression $m_{\mathrm{p}} c_{\mathrm{p,s}} \mathrm{d}T_{\mathrm{p}}/\mathrm{d}t$ for the change in internal energy instead of equation 6. That expression ignores the derivative of the particle's heat capacity and the derivative of the particle mass with respect to time. The heat capacity is temperature dependent and, hence, time dependent in the case of particle heating and cooling. The same applies to the particle mass in case of high laser fluences. This can have a significant influence on the calculated temperature decay and, therefore, on the derived particle diameter in case of the reverse process in fitting experimental LII signals.

Heat conduction

Heat conduction depends on the local gas-kinetic conditions that can be divided into three regimes: The free-molecular regime, the continuum regime and the transition regime.

1. Free-molecular regime

In the free-molecular regime, heat conduction is dominated by molecule-particle collisions. In the case of two concentric spheres and, hence, for a particle in an infinite gas bath, heat conduction can be described by

$$\dot{Q}_{\mathrm{cond,FM}} = \alpha \pi d_p^2 \frac{p}{8} \sqrt{\frac{8RT_{\mathrm{g}}}{\pi M_{\mathrm{g}}}} \frac{\left(\gamma^* + 1\right)}{\left(\gamma^* - 1\right)} \left(\frac{T_{\mathrm{p}}}{T_{\mathrm{g}}} - 1 \right) \tag{7}$$

where R is the universal gas constant, p is the gas pressure, α is the thermal accommodation coefficient, M_{g} is the molar mass of the gas, and T_{g} is the gas temperature. The average heat capacity ratio γ^* is defined by Filippov and Rosner [12] as

$$\frac{1}{\gamma^* - 1} = \frac{1}{T_p - T_g} \int_{T_g}^{T_p} \frac{dT}{\gamma - 1}. \tag{8}$$

In literature, the heat capacity ratio γ is often applied at constant gas-phase temperature. It has been pointed out by Liu et al. [13] that the average heat capacity ratio should be used if the temperature difference between the particle and the surrounding gas is large. Otherwise, the heat conduction will be underestimated, except for mono-atomic (noble) gases which have a temperature-independent heat capacity. In order to calculate the heat capacity ratio γ of the gas, the temperature-dependent heat capacity of the gas $c_{\mathrm{p,g}}$ is required. It is given by

$$c_{\mathrm{p,g}} = a_{\mathrm{c,g}} + b_{\mathrm{c,g}} T_{\mathrm{g}} + \frac{c_{\mathrm{c,g}}}{T_{\mathrm{g}}^2} \tag{9}$$

where $a_{\mathrm{c,s}}$, $b_{\mathrm{c,s}}$ and $c_{\mathrm{c,s}}$ are empirical constants [9].

2. Continuum regime

In the continuum regime, heat transfer between the particle and the surrounding gas is diffusion-controlled and, in contrast to the free-molecular regime, molecule-molecule collisions dominate over molecule-particle collisions. Compared to the free-molecular regime, however, molecule-particle collisions and, hence, heat conduction are strongly increased. As described by Filippov and Rosner [12] the heat flux can be expressed as

$$\dot{Q}_{\mathrm{cond,C}} = 2\pi d_{\mathrm{p}} \int_{T_{\mathrm{g}}}^{T_{\mathrm{p}}} k_{\mathrm{g}} \mathrm{d}T. \tag{10}$$

The thermal conductivity of the surrounding gas k_{g} is temperature dependent. In this work, the expression given by Michelsen [10] for air has been used:

$$k_{\mathrm{g}} = h_1 + h_2 T_{\mathrm{g}} \tag{11}$$

where h_1 and h_2 are empirical constants.

3.1. Transition regime: McCoy and Cha

A commonly-used heat conduction model for LII in the transition regime was given by Melton [3]. It is based on the work of McCoy and Cha [14] who derived the following expression for two concentric spheres in the transition regime:

$$\dot{Q}_{\mathrm{cond,Trans}} = \frac{2k_{\mathrm{g}}(T_{\mathrm{g}})\pi d_{\mathrm{p}}^2\left(T_{\mathrm{p}} - T_{\mathrm{g}}\right)}{\left(d_{\mathrm{p}} + G\lambda_{\mathrm{MFP}}\right)} \tag{12}$$

Here, the mean free path length is

$$\lambda_{\mathrm{MFP}} = \frac{k_{\mathrm{g}}(T_{\mathrm{g}})}{f(T_{\mathrm{g}})p}\left(\gamma(T_{\mathrm{g}})-1\right)\sqrt{\frac{\pi M_{\mathrm{g}} T_{\mathrm{g}}}{2R}}\,. \tag{13}$$

It has been pointed out by Liu et al. [13] that it is of high importance to use expression (13) in the case of the heat-conduction model of McCoy and Cha. In case of the often-used expression for hard spheres, i.e. $\lambda_{MFP} = k_B T_g / \left(\sqrt{2}\Sigma_g p\right)$, where k_{B} is the Boltzmann constant and Σ_{g} is the collisional cross-section of the gas molecules, large deviations occur for the heat-conduction rate using equation (12).
In (12) the factor G is

$$\frac{8f}{\alpha(\gamma+1)} \tag{14}$$

in which the Eucken factor f [15] is

$$f = \left(9\gamma - 5\right)/4\,. \tag{15}$$

The model of McCoy and Cha can be used for all heat-conduction regimes as it provides a smooth transition between the free-molecular and the continuum regime.

3.2. The transition regime: Fuchs' approach

Fuchs' approach [16,17] is based on the assumption that heat conduction from a particle to the surrounding gas in the transition regime can be divided into two zones. The boundary between the two zones is given by a sphere of thickness δ around the particle. This boundary layer δ is in the order of the mean free path length of the gas molecules.

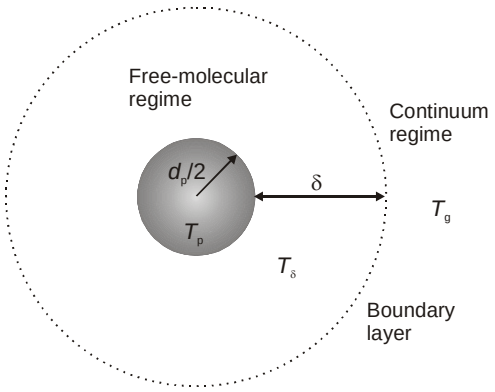

Figure 1. Heat-conduction for a spherical particle in the transition regime according to the model of Fuchs.

Inside this limiting sphere heat conduction is assumed to follow the mechanisms of the free-molecular flow, whereas outside the sphere heat conduction takes place according to the continuum regime as shown in Figure 1. The particle has the temperature T_{p}, the temperature inside the limiting sphere is T_δ and outside the sphere the gas has the temperature T_{g}.

The key point in using the Fuchs model is to find the values for the thickness of the boundary layer and the temperature inside this limiting sphere. Filippov and Rosner [12] describe the required equations to calculate δ and T_δ. The thickness of the limiting sphere can be calculated as

$$\delta = \frac{(d_{\mathrm{p}}/2)^3}{\lambda_{\mathrm{MFP},\delta}^2}\left(\frac{1}{5}\Lambda_1^5 - \frac{1}{3}\Lambda_2\Lambda_1^3 + \frac{2}{15}\Lambda_2^{5/2}\right) - \frac{d_{\mathrm{p}}}{2} \tag{16}$$

with the mean free path inside the sphere $\lambda_{\mathrm{MFP},\delta}$ and the coefficients

$$\Lambda_1 = 1 + \frac{\lambda_{\mathrm{MFP},\delta}}{d_{\mathrm{p}}/2};\quad \Lambda_2 = 1 + \left(\frac{\lambda_{\mathrm{MFP},\delta}}{d_{\mathrm{p}}/2}\right)^2 \tag{17}$$

The mean free path inside the sphere can be calculated with equation (13) with T_δ instead of T_{g}. Hence, with known pressure and molecular mass of the gas, δ is only a function of temperature in the boundary layer. The heat conduction inside the boundary layer is expressed by equation (7) and (8) with T_δ instead of T_{g}:

$$\dot{Q}_{\mathrm{cond,FM}} = \alpha\pi d_{\mathrm{p}}^2 \frac{p}{8}\sqrt{\frac{8RT_\delta}{\pi M_{\mathrm{g}}}}\frac{\left(\gamma^*+1\right)}{\left(\gamma^*-1\right)}\left(\frac{T_{\mathrm{p}}}{T_\delta} - 1\right) \tag{18}$$

Heat conduction outside the limiting sphere follows the model for the continuum regime. The 'particle diameter' is the diameter of the boundary layer, i.e. the radius is $\delta + d_{\mathrm{p}}/2$. If this value is inserted in equation (9) and T_{p} is substituted by T_δ one obtains for the heat conduction outside the sphere

$$\dot{Q}_{\mathrm{cond,C}} = 4\pi(\delta + d_{\mathrm{p}}/2)\int_{T_{\mathrm{g}}}^{T_\delta} k_{\mathrm{g}}\,\mathrm{d}T. \tag{19}$$

The next step is to obtain T_δ . As there are no sources or sinks of heat, equations (18) and (19) must be equal. With that relation T_δ and successively δ can be determined by solving the combination of expressions above numerically. Then, the heat conduction in the transition regime can be calculated by using either (18) or (19).

Vaporization

If the laser fluence is high and, therefore, the particles reach high temperatures, soot fragments can evaporate from the particle's surface. The amount of heat loss due to evaporation is given by the enthalpy of vaporization of soot, $\Delta H_{\mathrm{v,s}}$, the molar mass of the soot vapor $M_{\mathrm{v,s}}$ and the rate of mass loss $\mathrm{d}m_{\mathrm{p}}/\mathrm{d}t$:

$$\dot{Q}_{\mathrm{evap}} = \frac{\Delta H_{\mathrm{v,s}}}{M_{\mathrm{v,s}}}\frac{\mathrm{d}m_{\mathrm{p}}}{\mathrm{d}t} \tag{20}$$

The mass balance takes into account that the mass which evaporates from the particle will be in the gas phase:

$$\frac{\mathrm{d}m_\mathrm{p}}{\mathrm{d}t} = -\pi d_\mathrm{p}^2 N_\mathrm{v,s} \frac{M_\mathrm{v,s}}{N_\mathrm{A}} = J_\mathrm{evap} \tag{21}$$

Here, N_A is the Avogadro constant and $N_\mathrm{v,s}$ is the flux of molecules that leave the surface in the transition regime. The molecular flux in the transition regime can be expressed by the fluxes in the free-molecular regime, $N_\mathrm{FM,s}$, and the continuum regime, $N_\mathrm{C,s}$ [6]:

$$N_\mathrm{v,s} = \left(\frac{1}{N_\mathrm{FM,s}} + \frac{1}{N_\mathrm{C,s}} \right)^{-1} \tag{22}$$

The flux in the free-molecular regime can be expressed by

$$N_\mathrm{FM,s} = \beta \frac{p_\mathrm{v,s}}{k_\mathrm{B} T_\mathrm{p}} \sqrt{\frac{R T_\mathrm{p}}{2\pi M_\mathrm{v,s}}} \tag{23}$$

with the Boltzmann constant k_B, the vapor pressure $p_\mathrm{v,s}$ of the evaporating carbon species, and the evaporation coefficient β which is a number between 0 and 1 and can be used to adjust the efficiency of the evaporation. Usually, β is set to 1. The flux in the continuum regime can be expressed by

$$N_\mathrm{C,s} = 2 \frac{p_\mathrm{v,s}}{k_\mathrm{B} T_\mathrm{P}} \frac{\Gamma_\mathrm{v,s}}{d_\mathrm{p}} . \tag{24}$$

The diffusion coefficient of the soot vapor, $\Gamma_\mathrm{v,s}$, is given by Michelsen [10]:

$$\Gamma_\mathrm{v,s} = \frac{f k_\mathrm{B} T_\mathrm{p}}{4 \Sigma_\mathrm{v,s} p} \sqrt{\frac{R T_\mathrm{p}}{\pi M_\mathrm{v,s}}} \tag{25}$$

Here, $\Sigma_\mathrm{v,s}$ is the molecular cross section of the vapor. The question is which soot fragments evaporate from the surface. An overview on the evaporating carbon species in dependence on temperature is given by Leider et al. [18]. The dominant species above ~2000 K is C_3, though all species from C_1 – C_7 are present in the vapor in different concentrations. In LIISim, the species C_1 – C_7 are considered. The vapor pressure, molecular weight of the soot vapor and the enthalpy of vaporization are required as a function of the particle temperature. Smallwood and coworkers [19] derived these expressions from polynomial fits to data from Leider et al. The expressions are

$$p_\mathrm{v,s} = \exp\left(\sum_{i=0}^{5} p_i T_\mathrm{p}^i \right), \tag{26}$$

$$M_\mathrm{v,s} = \sum_{i=0}^{5} m_i T_\mathrm{p}^i , \tag{27}$$

$$\Delta H_\mathrm{v,s} = \sum_{i=0}^{5} h_i T_\mathrm{p}^i . \tag{28}$$

Finally, the molecular cross-sections of the vapor molecules are required. Michelsen [10] has given the molecular cross-sections for the species C_1 – C_{10}. For the present work, the data of Michelsen were fitted as a function of the molecular weight of the vapor. In that way, a polynomial expression for the molecular cross-section of the soot vapor could be derived

$$\Sigma_\mathrm{v,s} = \sum_{i=0}^{5} \sigma_i M_\mathrm{v,s}^i . \tag{29}$$

The coefficients for the polynoms (26) – (29) are listed in Table 1. The coefficients will result in SI units for $p_\mathrm{v,s}$, $M_\mathrm{v,s}$, $\Delta H_\mathrm{v,s}$ and $\Sigma_\mathrm{v,s}$.

i	p_i	m_i	h_i	s_i
0	–111.4	0.01718	205398	$1.8 \cdot 10^{-19}$
1	0.0906	$6.865 \cdot 10^{-7}$	736.6	$-1.857 \cdot 10^{-17}$
2	$-2.764 \cdot 10^{-5}$	$2.996 \cdot 10^{-9}$	–0.4071	$1.404 \cdot 10^{-15}$
3	$4.175 \cdot 10^{-9}$	$-8.595 \cdot 10^{-13}$	$1.199 \cdot 10^{-4}$	$-2.593 \cdot 10^{-14}$
4	$-2.488 \cdot 10^{-13}$	$1.049 \cdot 10^{-16}$	$-1.795 \cdot 10^{-8}$	$2.075 \cdot 10^{-13}$
5	0	0	$1.072 \cdot 10^{-12}$	$-6.667 \cdot 10^{-13}$

Table 1. Coefficients for the polynomial expressions of the vapor pressure, molecular mass of the vapor, enthalpy of vaporization and molecular cross-section of the vapor. The final values result in SI units.

Radiation

The heat loss due to radiation follows the Stefan-Boltzmann law. The emitted power over all wavelengths is

$$\dot{Q}_\mathrm{rad} = \pi d_\mathrm{p}^2 \theta \sigma_\mathrm{B} \left(T_\mathrm{p}^4 - T_\mathrm{g}^4 \right) \tag{30}$$

Here, σ_B is the Stefan-Boltzmann constant and θ the total emission coefficient. Assuming black body radiation, θ is set to 1. This is a simplified expression, as soot is not a perfect black body. The difference is, however, negligible at atmospheric or high pressure, as radiation has only a minor contribution to the heat loss under these conditions. At low pressures, however, radiation can be become the dominant heat loss mechanism and equation (30) should not be used.

LII signal

With the above described sub-models, the equations (1) and (2) are solved numerically with a fourth-order Runge-Kutta algorithm. This yields the temperature, the particle diameter, as well as the contributions of the different heat-loss mechanisms as a function of time. Finally, the particle temperature is turned into LII signal intensity using Planck's law since the particle radiation is near black-body radiation. Hence, the contribution to the signal from each particle in the detection volume is given by

$$S_\mathrm{LII} = 2\pi^2 h c^2 d_\mathrm{p}^2 \int_{\lambda_1}^{\lambda_2} \frac{\Omega(\lambda) \varepsilon(\lambda)}{\lambda^5 \left[\exp\left(hc / \lambda k_\mathrm{B} T_\mathrm{p} \right) - 1 \right]} \mathrm{d}\lambda \tag{31}$$

with the Planck constant h, the spectral response function of the detection system Ω, and the spectral

emissivity of soot ε. The emissivity is related to the absorption cross-section and is given by [10]

$$\varepsilon = \frac{4C_{\mathrm{abs}}}{\pi d_{\mathrm{p}}^2} = \frac{4\pi d_{\mathrm{p}} E(m)}{\lambda_{\mathrm{det}}} \tag{32}$$

The signal is integrated over the detection bandpass from λ_1 to λ_2.

Polydisperse particle sizes

In most cases, the particles within the probe volume are not monodisperse but polydisperse. This will have a significant impact on the LII signal as the cooling of the laser-heated particles strongly depends on the particle size. The temperature decay of a polydisperse ensemble of particles will be the integral of the individual cooling curves of the different particle sizes within the probe volume. It has been shown that for hydrocarbon flames at atmospheric and elevated pressure [20] the particles' size distribution follows a log-normal distribution given by

$$df = \frac{1}{\sqrt{2\pi}\, d_{\mathrm{p}} \ln\sigma_{\mathrm{g}}} \exp\left[-\frac{\left(\ln d_{\mathrm{p}} - \ln CMD\right)^2}{2\left(\ln\sigma_{\mathrm{g}}\right)^2} \right] \mathrm{d}d_{\mathrm{p}} \tag{33}$$

The distribution is characterized by the count median diameter *CMD* and the geometric width σ_{g}. *df* is the probability to find a particle size between d_{p} and d_{p} + $\mathrm{d}d_{\mathrm{p}}$. The distribution is not symmetric but has a long tail towards larger particles.

Aggregates

In real systems, nano-sized particles tend to stick together and form aggregates. The LII model modifications for aggregates were presented for the first time by Snelling et al. [21] and were improved by Liu and coworkers [22,23]. A soot particle within an aggregate cools down slower than an isolated, single particle because a primary particle inside an aggregate is shielded by surrounding primary particles. The sub-model in LIISim that includes aggregation is taken from the work of Liu et al. and is described in detail in [23]. In LIISim, a monodisperse aggregate size of a given number of primary particles is used, whereas the size distribution of the primary particles can be chosen to be mono- or polydisperse. The aggregate model can be used in the free molecular, the continuum, and in the transition regime. In the transition regime, the Fuchs model for heat conduction is used. The aggregate model does not take into account the effect of aggregation on the vaporization term and, therefore, can only be used in the case of low laser fluences when vaporization is negligible.

LIISim program

The different models described above are implemented as a C code. This program is called LIISim and is executed from the command line. LII signals can be simulated for different initial conditions which are given to the program by ASCII files.

Experimental LII data can be fitted by LIISim as well. With the chosen initial physical parameters and the selected heat-conduction model the particle diameter or the mean particle diameter and the width of a log-normal particle-size distribution are determined by a Levenberg-Marquardt non-linear least-squares fitting algorithm. The peak particle temperature is obtained from two-color LII data as described in the next section.

LIISim web interface

A web interface of LIISim is available at the site http://www.liisim.com. Both the modeling part and the fitting part are accessible by the web interface.

Modeling LII signals

In the modeling part, LII signals can be modeled using different initial settings. The user can select between general settings like the choice between mono- or polydisperse particles, single particles or aggregates and different heat conduction models as described in the previous sections.

The physical input parameters can be set, which are divided into the sections absorption parameters, particle properties, gas-phase properties, and the detection bandpass. Parameters like the soot absorption function, laser fluence, gas-phase temperature, gas pressure, and the accommodation coefficient can be set here. If the LII-signal decay without heat-up should be modeled, the laser fluence must be set to zero and the initial particle temperature should be set to the desired value.

After the calculation is performed, the LII signal will be shown as a graph and the resulting data file can be downloaded. In the data file, the time history of the LII signal, the particle temperature, the particle diameter, as well as the contributions of the different heat-loss mechanisms are listed. All values are given in SI units.

Fitting experimental LII signals

In the fitting part, individual experimental LII signal traces can be uploaded. The fit uses a two-color LII method: Two time-resolved LII signals detected at two different wavelengths λ_1 and λ_2 are taken to calculate the peak particle temperature T_{p}^0 the particles reach after laser heat-up. The peak temperature is calculated from the peak signals $S_{\mathrm{p}}(\lambda_1, T_{\mathrm{p}}^0)$ and $S_{\mathrm{p}}(\lambda_2, T_{\mathrm{p}}^0)$ according to

$$T_p^0 = \frac{hc}{k_B}\left(\frac{1}{\lambda_2} - \frac{1}{\lambda_1}\right) \cdot \left[\ln\left[\frac{S_p(\lambda_1, T_p^0)}{S_p(\lambda_2, T_p^0)} \frac{K_2(\lambda_2)}{K_1(\lambda_1)} \frac{\varepsilon(\lambda_2)\lambda_1^{\,5}}{\varepsilon(\lambda_1)\lambda_2^{\,5}}\right]\right]^{-1} \tag{34}$$

where c is the speed of light, S_p is the detected emission signal from the particles at the two detection wavelengths, and K_1 and K_2 are constants that take into account the spectral sensitivity of the detectors and the detection filters at the two wavelengths. The ratio of the emissivities $\varepsilon(\lambda_2)/\varepsilon(\lambda_1)$ is approximated by λ_1/λ_2 assuming that $E(m)$ is constant between the two

wavelengths. The peak particle temperature is used as start temperature for the fit. Then, the experimental LII-signal decay is fitted by LIISim with the particle diameter as free fit parameter. A graph of the experimental signal and the best fit will be returned and the data file containing the fit results can be down-loaded. Additional information on the two-color LII method can be found in [9].

It should be noted that the fit procedure can only be used for LII signals recorded at low laser fluences, i.e. the soot temperature is well below the vaporization threshold. Because the vaporization sub-model of LIISim is related to uncertainty, the fit will result in poor results for LII signals recorded at high laser fluences. Care should be taken to fill in all the required input data of the conditions at which the LII signals were taken, e.g. the gas-phase temperature, gas pressure, etc. A calibration constant for the two-color LII setup is required for the respective experiment, i.e. the ratio of K_1/K_2 to ensure the correct calculation of the peak particle temperature. The calibration constant must be entered on the web interface. Information about the required format and quality of the uploaded experimental LII signals are given in detail on the web site. The careful reading of all additional information on the web site is of utmost importance for a correct use of the LIISim fitting procedure.

Conclusion

We presented a computer program that simulates the heat-up and cooling of nano-sized soot particles by a pulsed laser. The program, called LIISim, includes several recent developments in modeling LII, like the choice between mono- or polydisperse particles, single or aggregated particles, and different heat-conduction models.

For the first time, an LII model is made available to the scientific community by a web interface. This web interface allows to use LIISim as a simulation tool or as a tool to fit individual LII-signal traces. The web interface of LIISim is available at the web site http://www.liisim.com.

Acknowledgements

The financial support of the Deutsche Forschungs-gesellschaft (DFG) is gratefully acknowledged. The authors would like to thank Dr. Wolfgang Bessler, IWR, University of Heidelberg, for his support in web interface programming.

References

1. Schulz, C., Kock, B. F., Hofmann, M., Michelsen, H., Will, S., Bougie, B., Suntz, R., and Smallwood, G., *Appl. Phys. B* 83:333 (2006).
2. Michelsen, H. A., Liu, F., Kock, B. F., Bladh, H., Boiarciuc, A., Charwath, M., Dreier, T., Hadef, R., Hofmann, M., Reimann, J., Will, S., Bengtsson, P.-E., Bockhorn, H., Foucher, F., Geigle, K.-P., Mounaïm-Rousselle, C., Schulz, C., Stirn, R., Tribalet, B., and Suntz, R., *Appl. Physics. B* (in press).
3. Melton, L. A., *Appl. Opt.* 23:2201-2208 (1984).
4. Snelling, D. R., Liu, F., Smallwood, G. J., and Gülder, Ö. L. "Evaluation of the nanoscale heat and mass transfer model of LII: Prediction of the excitation intensity," in *34th National Heat Transfer Conference* (Pittsburgh, 2000).
5. Will, S., Schraml, S., Bader, K., and Leipertz, A., *Appl. Opt.* 37:5647-5658 (1998).
6. Hofeldt, D. L., *SAE Technical Paper Series No. 930079* (1993).
7. Bladh, H. and Bengtsson, P.-E., *Appl. Phys. B* 78:241-248 (2004).
8. Mewes, B. and Seitzman, J. M., *Appl. Opt.* 36:709-717 (1997).
9. Kock, B. F., Tribalet, B., Schulz, C., and Roth, P., *Comb. and Flame* 147:79-92 (2006).
10. Michelsen, H. A., *J. Chem. Phys.* 118:7012-7045 (2003).
11. Kerker, M., *The Scattering of Light and other Electromagnetic Radiation* (Academic, New York, 1969).
12. Filippov, A. V. and Rosner, D. E., *Int. J. Heat and Mass Transfer* 43:127-138 (2000).
13. Liu, F., Daun, K. J., Snelling, D. R., and Smallwood, G. J., *Appl. Phys. B* 83:355 (2006).
14. McCoy, B. J. and Cha, C. Y., *Chem. Eng. Science* 29:381-388 (1974).
15. Chapman, S. and Cowlings, T. G., *Mathematical Theory of Non-Uniform Gases* (Cambridge U.P., London, 1970).
16. Fuchs, N. A., *Geophys. Pura Appl.* 56:185-193 (1963).
17. Fuchs, N. A., *The Mechanics of Aerosols* (Pergamon Press, Oxford, 1964 (Dover Publications, New York, 1989)).
18. Leider, H. R., Krikorian, O. H., and Young, D. A., *Carbon* 11:555-563 (1973).
19. Smallwood, G. J., Snelling, D. R., Liu, F., and Gülder, Ö. L., *J. Heat Transfer* 123:814-818 (2001).
20. Heidermann, T., Jander, H. H., and Wagner, H. G., *Phys. Chem. Chem. Phys.* 1:3497-3502 (1999).
21. Snelling, D. R., Liu, F., Smallwood, G. J., and Gülder, Ö. L., *Combust. Flame* 136:180-190 (2004).
22. Liu, F., Smallwood, G. J., and Snelling, D. R., *J. Quant. Spectros. Radiat. Transfer* 93:301-312 (2005).
23. Liu, F., Yang, M., Hill, F. A., Snelling, D. R., and Smallwood, G. J., *Appl. Phys. B* 83:383 (2006).